

1 Supplemental materials for

2

3 **RADICAL: a rationally designed ion channel activated by ligand for**  
4 **chemogenetics**

5 Heng Zhang <sup>1,2,5</sup>, Zhiwei Zheng <sup>3,4,5</sup>, Xiaoying Chen <sup>1,2</sup>, Lizhen Xu <sup>1,2</sup>, Chen Guo <sup>3,4</sup>,  
6 Jiawei Wang <sup>1,2</sup>, Yihui Cui <sup>3,4\*</sup>, Fan Yang <sup>1,2\*</sup>

7 <sup>1</sup> Liangzhu Laboratory, Zhejiang University Medical Center, Hangzhou, Zhejiang 311121,  
8 China.

9 <sup>2</sup> Kidney Disease Center of the First Affiliated Hospital and Department of Biophysics,  
10 Zhejiang University School of Medicine, Hangzhou, Zhejiang Province, China

11 <sup>3</sup> Department of Neurobiology, Department of Neurology of Sir Run Run Shaw Hospital,  
12 Zhejiang University School of Medicine, 310058, Hangzhou, China

13 <sup>4</sup> NHC and CAMS Key Laboratory of Medical Neurobiology, MOE Frontier Science Center  
14 for Brain Research and Brain-Machine Integration, School of Brain Science and Brain  
15 Medicine, Zhejiang University, 310058 Hangzhou, China

16 <sup>5</sup> These authors contributed equally to this work

17 \*Correspondence should be addressed to:

18 Fan Yang (fanyanga@zju.edu.cn), Yihui Cui (yihuicui@zju.edu.cn)

19

## 20 **Materials and methods**

### 21 **Chemicals**

22 Cyclohexanol (CHOXL) were purchased from Sigma Aldrich (MCE) and Sangon  
23 Biotech. Menthol was purchased from TCI Shanghai, Capsaicin was purchased from  
24 MCE, GSK1016790A was purchased from Topscience, AITC, 2-APB were purchased  
25 from Sigma-Aldrich, and A-967079 was purchased from Tocris. All compounds  
26 except additional statement were dissolved in DMSO.

### 27 **Animals**

28 Male adult (7-15 weeks of age) C57BL/6J mice (SLAC) were used for this project.  
29 Mice were housed 4-5 per cage under a 12-h light-dark cycle (light on from 7 a.m. to  
30 7 p.m.) with ad libitum food and water. All animal studies and experimental  
31 procedures were approved by the Animal Care and Use Committee of the animal  
32 facility at Zhejiang University.

### 33 **Cell culture**

34 HEK293T cells are cultured using DMEM medium contained 10% FBS in a cell  
35 incubator with 5% CO<sub>2</sub> at 37 °C. Plasmids of murine TRPV1, TRPV2, TRPV3,  
36 TRPV4, TRPM8 and human TRPA1, Kv4.2, Nav1.7 and hERG channels are labeled  
37 with YFP or GFP as indicators for subsequent electrophysiological recordings. cDNA  
38 constructs of ion channels or TRPM8 mutants were transiently transfected with  
39 Lipofectamine 2000 (Invitrogen, Carlsbad, CA). 18-24 h after transient transfection,  
40 electrophysiological recordings were performed.

41 Site mutations of TRPM8 channel were generated by Fast Mutagenesis Kit (Takara  
42 Bio). All mutations were confirmed by sequencing.

### 43 **Molecular docking of CHOXL to TRPM8 channel and generation of I846F** 44 **mutant model**

45 The molecular docking was performed as previously described (Yang et al., 2015). In  
46 brief, RosettaLigand procedure of Rosetta program suite version 2019 was used to  
47 perform molecular docking of CHOXL to TRPM8 and generate TRPM8 mutant  
48 model (Meiler and Baker, 2006), and Monte Carlo algorithm was employed for  
49 sampling. The three-dimensional 3D conformation of CHOXL was generated by  
50 Frog2 server (Miteva et al., 2010). The structure of TRPM8 (PDB ID: 6NR3) was  
51 relaxed by Relax application in Rosetta program suite.

52 The relaxed structure of wildtype TRPM8 was used as input file to generate model of  
53 TRPM8 I846F mutant in Rosetta Backrub application (Smith and Kortemme, 2008).  
54 100 models were generated and the model with lowest energy was selected for further  
55 relax. The best structure model with lowest energy of I846F mutants was relaxed as  
56 described above. 100 relaxed models were generated and models with the lowest  
57 energy were chosen as candidates for the docking step.

58 CHOXL was put in the menthol-binding pocket of WT TRPM8 and I846F mutant, the  
59 top 10 models with lowest binding energy from 30000 generated models were chosen  
60 for further analysis. Rosetta's Residue\_energy\_breakdown application was used to  
61 extract binding energies between CHOXL and TRPM8.

## 62 **Electrophysiology**

63 Patch-clamp recordings were carried out with a HEKA EPC10 amplifier controlled by  
64 PatchMaster software (HEKA). Patch pipettes were prepared from borosilicate glass  
65 and fire-polished to resistance of 3~8 M $\Omega$  by P-97 puller. For whole-cell recordings  
66 of TRPM8 channel and AISC channels, bath solution contained 145 mM NaCl, 2 mM  
67 KCl, 2 mM MgCl<sub>2</sub>, 1.5 mM CaCl<sub>2</sub>, 10 mM HEPES, 10 mM glucose were adjusted to  
68 pH 7.2 ~ 7.4 with NaOH; pipette solution contained 135 mM CsCl, 1 mM MgCl<sub>2</sub>, 2  
69 mM CaCl<sub>2</sub>, 10 mM HEPES, 5 mM EGTA were adjusted to pH 7.2 ~ 7.4 with CsOH.  
70 For solution with pH 5.0, HEPES was replaced by MES. To obtain icilin-induced  
71 TRPM8 current, a solution containing 135 mM NaCl, 0.5 mM CaCl<sub>2</sub>, 10 mM glucose  
72 and 3 mM HEPES was used as pipette and bath solution. Whole-cell recordings were  
73 performed at  $\pm$ 80 mV. Current was sampled at 10 kHz and filtered at 2.9 kHz.

74 For cation permeability experiment, the bath solution and pipette solution contained  
75 145 mM NaCl, 10 mM HEPES and 10 mM glucose (pH 7.4 with NaOH). After the  
76 whole-cell configuration was obtained in bath solution, the external Na<sup>+</sup> was changed  
77 to 145 mM K<sup>+</sup> and 145 mM NMDG<sup>+</sup> (pH 7.4). For Ca<sup>2+</sup> permeability measurement,  
78 external Na<sup>+</sup> was replaced with 100 mM NMDG and 30 mM CaCl<sub>2</sub>. Cation  
79 permeability was estimated by the shift of reversal potential relative to Na<sup>+</sup>, which can  
80 be obtained from voltage ramp recordings (voltage ramp from -120 mV to 120 mV in  
81 360 ms). Monovalent cation permeability and Ca<sup>2+</sup> permeability was calculated from  
82 the equation (1) and (2), respectively (Valera et al., 1994),(Xu et al., 2002).

83 
$$P_X/P_{Na} = \{[Na^+]_o/[X]_o\} \{\exp((F/RT)(V_X - V_{Na}))\} \quad (1)$$

84 
$$P_{Ca}/P_{Na} = \{[Na^+]_o/4[Ca^{2+}]_o\} \{\exp((F/RT)(V_{Ca} - V_{Na}))\} \{1 + \exp(FV_{Ca}/RT)\} \quad (2)$$

85 where  $[X]_o$  is defined as the extracellular concentration of the monovalent cations,  $P$   
86 is defined as the permeability of the ion.  $F$  is Faraday's constant,  $R$  is the gas constant,  
87  $T$  is temperature in Kelvins and  $V$  is the reversal potential for the cation ions.

88 For whole-cell recordings of TRPV1, TRPV2, TRPV3, TRPV4, and TRPA1 channels,  
89 both bath and pipette solutions contained (in mM): 130 NaCl, 10 glucose, 0.2 EDTA,  
90 and 3 HEPES (pH 7.2 ~ 7.4, adjusted with NaOH). Whole-cell recordings were  
91 performed at  $\pm 80$  mV. Current was sampled at 10 kHz and filtered at 2.9 kHz. For  
92 whole-cell recordings of Nav1.7 channels, bath solution contained (in mM): 145  
93 NaCl, 2 KCl, 2 MgCl<sub>2</sub>, 1.5 CaCl<sub>2</sub>, 10 HEPES, 10 glucose (pH 7.2 ~ 7.4, adjusted with  
94 NaOH); pipette solution contained (in mM): 140 CsF, 10 NaCl, 1 EGTA and 10  
95 HEPES (pH 7.3, adjusted with CsOH). Current traces were evoked by a 200 ms step  
96 depolarization to  $-10$  mV or  $0$  mV from a holding potential of  $-80$  mV every 2 s to  
97 avoid the fast desensitization of Nav channels. For whole-cell recordings of Kv4.2  
98 channels, bath solution contained (in mM): 145 NaCl, 2 KCl, 2 MgCl<sub>2</sub>, 1.5 CaCl<sub>2</sub>, 10  
99 HEPES, 10 glucose (pH 7.2 ~ 7.4, adjusted with NaOH); pipette solution contained  
100 (in mM): 135 KCl, 2 MgCl<sub>2</sub>, 1 EGTA, 10 HEPES and 2 Na<sub>2</sub>ATP (pH 7.3, adjusted  
101 with KOH). To obtain the current of Kv4.2 channel, the membrane potential was  
102 clamped at  $-60$  mV for 10 ms and switched to voltage stepping from  $-60$  mV to  $+60$   
103 mV with a 20-mV interval for 300 ms, and then switched to  $-60$  mV for 10 ms.

104 Currents were sampled at 10 kHz and filtered at 2.9 kHz.

105 All recordings were performed at room temperature (25 °C). A gravity-driven system  
106 (RSC-200, Bio-Logic) with freely rotated perfusion tubes was used for the perfusion  
107 of peptide or ligands. Bath and ligand-contained solutions were delivered through  
108 separate tubes to minimize the mixing of solutions. Patch pipette holding cells was  
109 placed in front of the perfusion tube outlet for perfusion.

### 110 **Calcium imaging**

111 Calcium imaging was conducted as previously described (Zhang et al., 2023). In brief,  
112 HEK293T cells expressing TRPM8 or TRPM8 mutants were incubated with 2  $\mu$ M  
113 Fluo-4 AM (Thermo Fisher) in 2 mM calcium Ringer's solution (140 mM NaCl, 5  
114 mM KCl, 2 mM MgCl<sub>2</sub>, 2 mM CaCl<sub>2</sub>, 10 mM glucose, and 10 mM HEPES, pH 7.4).  
115 Fluorescence images of HEK293T cells were acquired with Nikon Eclipse Ti2  
116 microscope with optiMOS charge-coupled device camera controlled by the Ocular  
117 Software (Molecular Devices). Fluo-4 AM was excited at 500/20-nm excitation, and  
118 fluorescence emission was detected at 535/30-nm. Fluorescence images were  
119 analyzed with Fiji software and Office Excel.

### 120 **Cell death assay**

121 Cell death was Cell death assay was performed as previous described (Zhang et al.,  
122 2019; Zhang et al., 2023). In brief, HEK293T cells were seeded in six-well plates and  
123 randomly divided into different groups after transfection. Then CHXOL was  
124 incubated for 18 h before the determination of cell death. Hoechst 33258 (Sangon

125 Biotech) was used to labeled all cell nuclei and propidium iodide (PI) (Sangon  
126 Biotech) was used to labeled nuclei of dead cells. In each group, five images were  
127 randomly taken under a microscope (STELLARIS8, Leica, German). Cell death ratio  
128 was represented by the average of the percentage of dead cells (PI-labeled cells over  
129 Hoechst-labeled cells) from five images. Fiji software was used to count cells.

### 130 **Calculation of $\Delta H$ and $\Delta S$**

131 Calculation of  $\Delta H$  and  $\Delta S$  was performed as previously described(Yang et al., 2020;  
132 Xu et al., 2021). To calculate the change of enthalpic ( $\Delta H$ ) and entropic ( $\Delta S$ ) due to  
133 the temperature-driven transition of TRPM8, we constructed Van't Hoff plots and  
134 fitted them to the equation  $\ln K_{eq} = -\Delta H/RT + \Delta S/R$ , whereby R represents the gas  
135 constant, T represents the temperature in Kelvin,  $K_{eq}$  represents the equilibrium  
136 constant measured from the cold-driven TRPM8 open probability,  $K_{eq} = P_o/(1-P_o)$ .  
137 The TRPM8 open probability induced by cold was calculated by noise analysis.

### 138 **Stereotaxic Surgery and Virus Injection**

139 For Stereotaxic surgery, mice (7-8 weeks) were anaesthetized with Pentobarbital  
140 NEMBUTAL (100 mg/kg, Sigma-Aldrich). Viruses were bilaterally injected by a  
141 glass pipette mounted on a stereotactic frame into IL ( $\pm 0.30$  mm ML, +1.95 mm AP, -  
142 2.30 mm DV) and VTA ( $\pm 0.5$  mm ML, -3.04 mm AP, -4.30 mm DV). Volumes of  
143 virus were 1  $\mu$ L per side, infused at a rate of 100 nL/min. The injection pipette was  
144 withdrawn from the brain 10 min after the infusion. After surgery, mice were  
145 recovered from anesthesia on a heat pad. The viral injection sites were verified by

146 post immunohistochemistry experiment as we demonstrated with schematics in Fig.  
147 S4.

#### 148 **Fear conditioning test**

149 3 weeks after surgery, all mice were handled for three days before behavioral assays  
150 for 5 min per day. For cued fear conditioning experiments, mice were placed in a  
151 chamber with a grid floor connected to a shock generator (Coulbourn instruments).  
152 Three minutes after being placed in the chamber, mice were exposed to 30-s tones (3  
153 kHz, 80 dB) co-terminating with a 2-s foot shock (0.6 mA) for three times at pseudo-  
154 random inter-trial intervals (~2 min average). The chamber was cleaned with 75%  
155 ethanol at the end of each trial. The next day for fear extinction, mice were placed in a  
156 different context (floor and walls were changed and white vinegar was sprayed in the  
157 chamber). First, mice were injected (i.p.) with CHXOL (100 mg/kg or 10 mg/kg) or  
158 saline before extinction test. After 30 min, mice were exposed to 10 tones to undergo  
159 fear extinction. On day 3, mice were placed in the same environment as in day 2 and  
160 were exposed to one presentation of the tone. Behavior was recorded using digital  
161 video cameras. Freezing was scored by the fear conditioning software (FreezeFrame).

#### 162 **Open field test**

163 Mice were placed in the center of an area (45 cm × 45 cm × 45 cm) in a room with  
164 dim light for 10 min. A video camera positioned directly above the arena was used to  
165 track the movement of each animal (Any-maze, Stoelting). For mice with injection of  
166 pLenti-GfaABC1D-mCherry-P2A-mTRPM8(I846F-I985K)-WPRE virus in VTA

167 astrocytes, mice received an injection of CHXOL (100 mg/kg or 10 mg/kg) 30  
168 minutes before the beginning of the test.

### 169 **Slice preparation**

170 Mice were anaesthetized with 1% pentobarbital NEMBUTAL (100 mg/kg), perfused  
171 with 200 ml ice-cold artificial cerebrospinal fluid (ACSF, oxygenated with 95% O<sub>2</sub>,  
172 5% CO<sub>2</sub>) containing (in mM): 210 sucrose, 125 NaCl, 2.5 KCl, 25 NaHCO<sub>3</sub>, 1.25  
173 NaH<sub>2</sub>PO<sub>4</sub>, 1 MgCl<sub>2</sub>, 1 CaCl<sub>2</sub>, 25 glucose and 1 sodium pyruvate. After decapitation,  
174 the brains were transferred rapidly into ice-cold oxygenated ACSF. 300 μm thickness  
175 coronal slices, or sagittal slices if specified, containing the IL were sectioned in cold  
176 ACSF with a Leica VT1200S vibratome, and incubated in a recovery chamber  
177 containing ACSF (in mM): 125 NaCl, 2.5 KCl, 25 NaHCO<sub>3</sub>, 1.25 NaH<sub>2</sub>PO<sub>4</sub>, 1 MgCl<sub>2</sub>,  
178 1 CaCl<sub>2</sub>, 25 glucoses at 32 °C. ACSF was continuously gassed with 95% O<sub>2</sub>, 5% CO<sub>2</sub>.  
179 Slices were allowed to recover for at least 1 h before recordings and then transferred  
180 to room temperature.

### 181 ***In vitro* electrophysiology**

182 Whole cell patch clamp recordings were made from neurons in the IL under an  
183 upright microscope (BX51WI, Olympus). All recordings were performed at 34 °C  
184 using a temperature control system and slices were continuously superfused at 2-3  
185 mL/min with the extracellular solution. The patch pipettes were pulled with a pipette  
186 puller (PC-100, Narishige) from borosilicate glass (Sutter Instrument) and had a  
187 resistance of 5-6 MΩ. Electrophysiological recordings were made using a MultiClamp

188 700B amplifier and pCLAMP 10.6 software (Axon Instruments). Signals were  
189 amplified, filtered at 2 kHz and sampled at 10 kHz using Digidata 1550B. The series  
190 resistance and capacitance were compensated automatically after a stable Gigaseal  
191 was formed. Experiments were discarded if a change in series resistance was above  
192 20%.

193 Patch pipettes were filled with internal solution containing (in mM) 127 K-gluconate,  
194 13 KCl, 4 Mg<sub>3</sub>-ATP, 0.3 Na<sub>3</sub>-GTP, 0.3 EGTA, 10 HEPES and 10 Na-phosphocreatine  
195 (pH = 7.25). The external ACSF solution contained (in mM) 125 NaCl, 2.5 KCl, 25  
196 NaHCO<sub>3</sub>, 1.25 NaH<sub>2</sub>PO<sub>4</sub>, 1 MgCl<sub>2</sub>, 1 CaCl<sub>2</sub> and 25 glucoses. The resting membrane  
197 potential (RMP) of a neuron was obtained under current clamp (I = 0 pA), and the  
198 action potential (AP) was measured by injecting a series of current pulses (500 ms  
199 duration, -100 to 200 pA intensity with an increment of 20 pA). CHXOL (0.1 mM or  
200 1 mM) was dissolved in DMSO and added in ACSF with a final concentration of  
201 0.02%. The effect of CHXOL was recorded after 4 min of drug perfusion.

## 202 **Statistical analysis**

203 All statistical data are shown as mean ± S.E.M. Paired t-test was used to analyze the  
204 statistical significance between two groups in GraphPad Prism 7.0 software  
205 (GraphPad Inc., La Jolla, CA). For more than two groups, one-way ANOVA was  
206 used. n.s. indicates no significance. \*, \*\*, and \*\*\* indicate  $p < 0.05$ ,  $p < 0.01$ , and  $p <$   
207  $0.001$ , respectively. EC<sub>50</sub> was obtained from the fitting curves to the concentration-  
208 response relationship using Hill Equation in Igor Pro 5.0 software.

209

210 **Supplementary Figure Legends**

211 **Fig. S1 Selectivity of CHXOL on ion channels**

212 **A-K**, The effect of 1 mM or 3 mM CHXOL on TRPV1, TRPV2, TRPV3, TRPV4,  
213 TRPA1, Kv4.2, ASIC1a, ASIC2a, ASIC3, Nav1.7 and hERG channels. 1, bar graph of  
214 activation of CHXOL on these channels. (n = 3-8).

215 **Fig. S2 CHOXL did not affect RMPs and intrinsic excitability of IL neurons**

216 **A-C**, Resting membrane potential (RMP) of IL neuron after perfusion with bath or 10  
217 mM CHXOL. (**A**, n = 6, mice = 2, paired t-test, p > 0.999; **B-C**, n = 5, mice = 2,  
218 Wilcoxon test, P = 0.0635).

219 **Fig. S3 The effect of CHOXL on TRPM8 I846 mutants with different sizes of side**  
220 **chain at the membrane potential of  $\pm 80$  mV.**

221 **Fig. S4 CHXOL induced limited calcium influx by activating I846F-I985K**

222 **mutant. A**, Fluorescence images of HEK293T cells expressing I846F-I985K mutant  
223 in response to CHXOL or ionomycin, scale bar = 25  $\mu$ m. **B**, The normalized  
224 fluorescence intensity of HEK293T cells expressing I846F-I985K mutant (n = 4). **C**,  
225 Hoechst and PI staining of HEK293T cells expressing WT TRPM8 channel or I846F-I985K  
226 mutant in the presence or absence of CHXOL. Hoechst labelled nuclei of all cells and  
227 PI labelled nuclei of dead cells, scale bar=100  $\mu$ m. **D**, Cell death ratio calculated from  
228 panel **c**.

229 **Fig. S5 Concentration-response of icilin on WT TRPM8 and I846F-I985K**

230 **mutant. A and B**, Concentration-response of CHOXL on WT TRPM8 channel and

231 TRPM8 I846F-I985K mutant at  $\pm 80$  mV, respectively. **C**, Concentration-response  
232 curves of CHOXL on WT TRPM8 channel and TRPM8 I846F-I985K mutant ( $n = 6$ ).  
233 **D**, Representative cold activation of TRPM8 and TRPM8 mutants. **E**, Van't Hoff plots  
234 for the cold-activated TRPM8 currents shown in **D**. Dotted lines represent fits of the  
235 Van't Hoff equation, from which  $\Delta H$  and  $\Delta S$  are estimated. **F** and **G**, Measured  $\Delta H$   
236 values and  $\Delta S$  values, respectively. ( $n = 4-7$ ; mean  $\pm$  SEM; N.S. by one-way  
237 ANOVA).

238 **Fig. S6. The information of plasmid carried by Lenti-virus and verification of the**  
239 **insertion of TRPM8 mutants.**

240 **A**, Information of plasmid carried by Lenti-virus. **B**, Representative successful  
241 insertion of mTRPM8 mutant as validated by enzymatic digestion (SpeI and NotI) and  
242 DNA electrophoresis. The band in red box corresponded to mTRPM8 mutant.

243 **Fig. S7. Viral injection sites for electrophysiological and behavioral experiments**

244 Schematics of the corresponding brain regions in which viruses were detected. Each  
245 color represents the expression from a single mouse that was used for  
246 electrophysiological and behavioral experiments.

Fig. S1

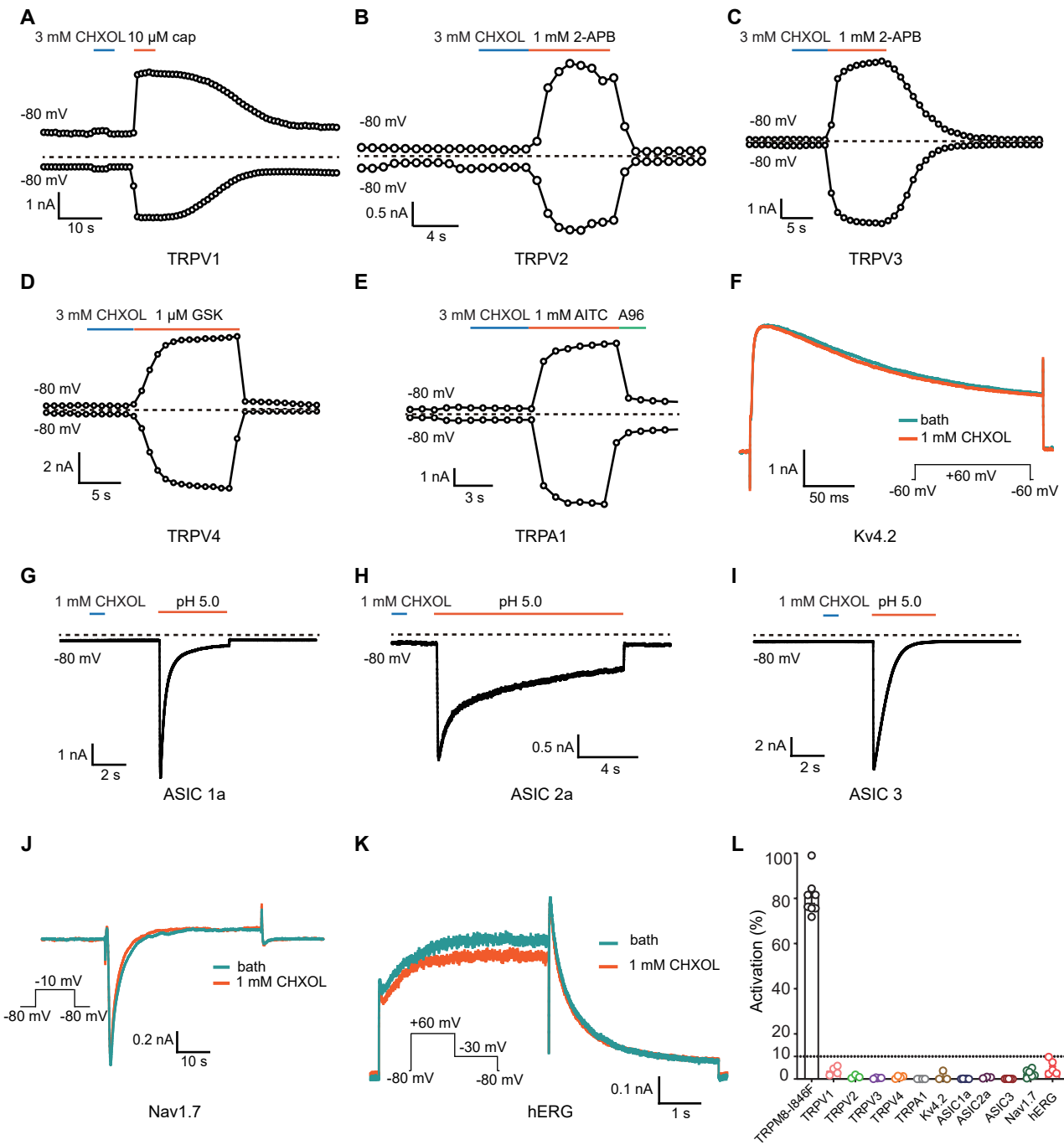


Fig. S2

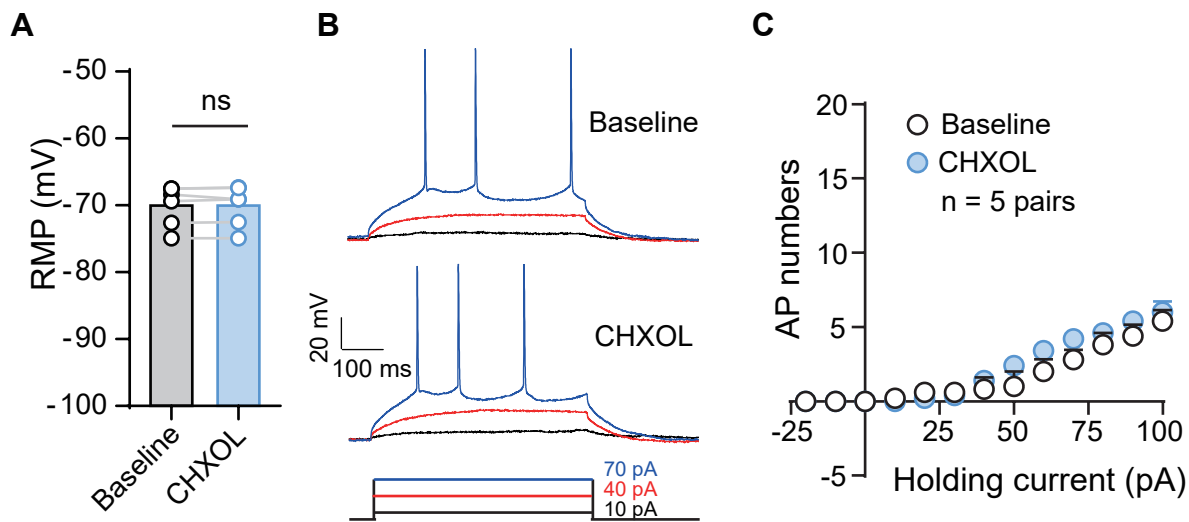


Fig. S3

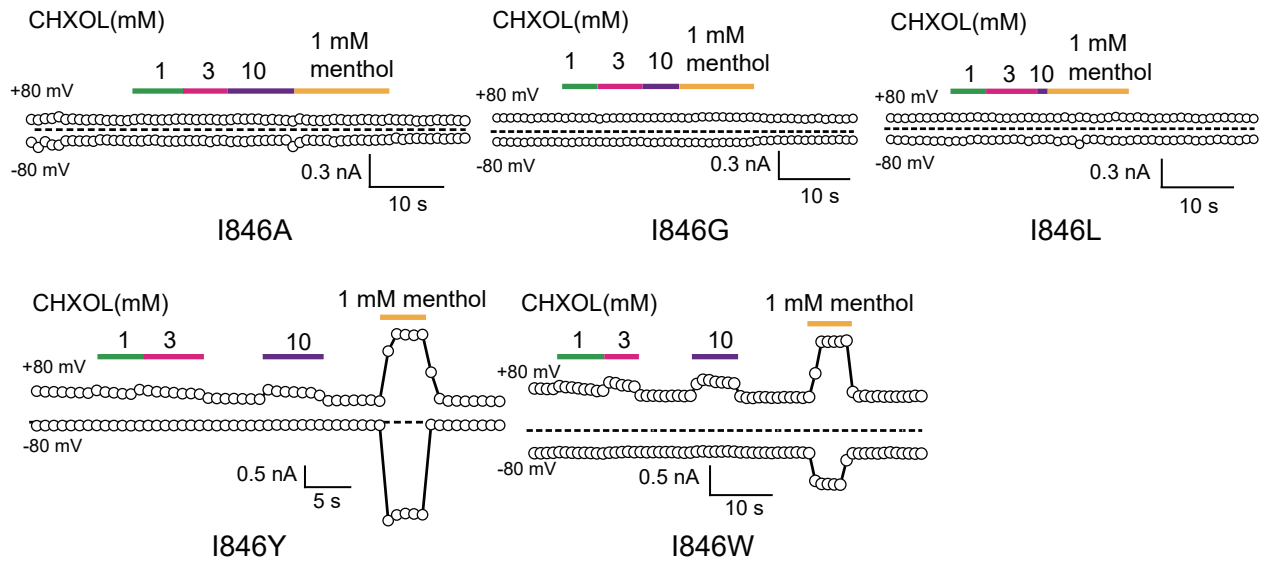


Fig. S4

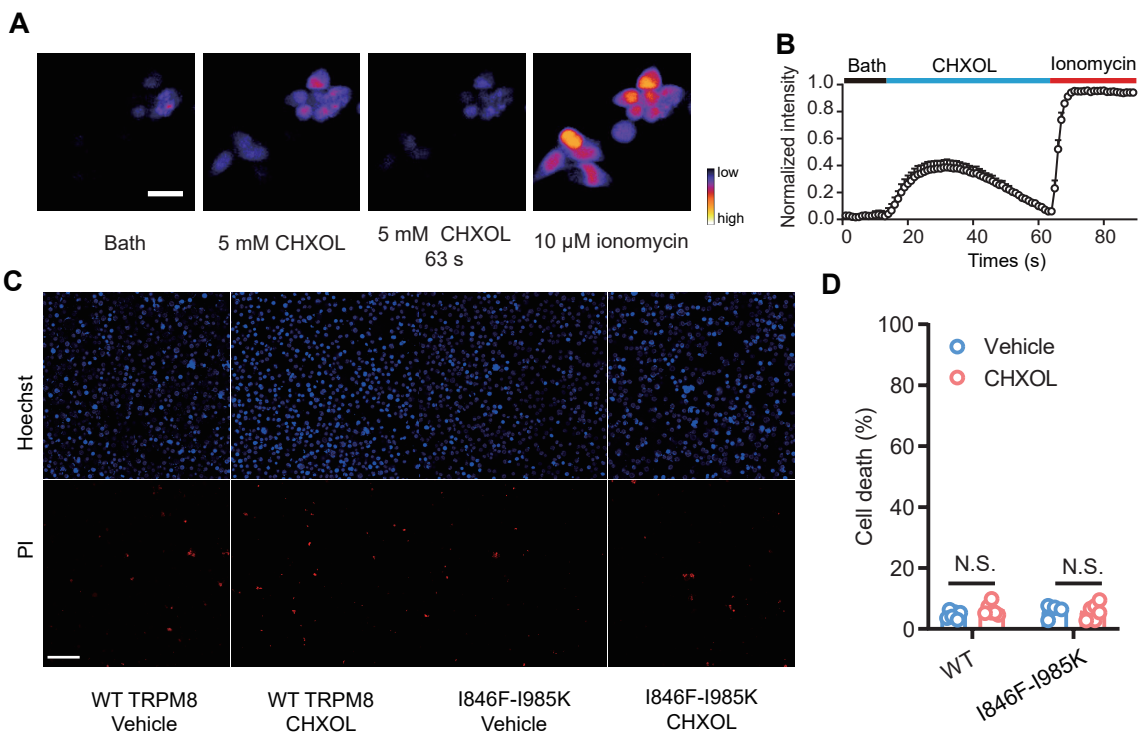


Fig. S5

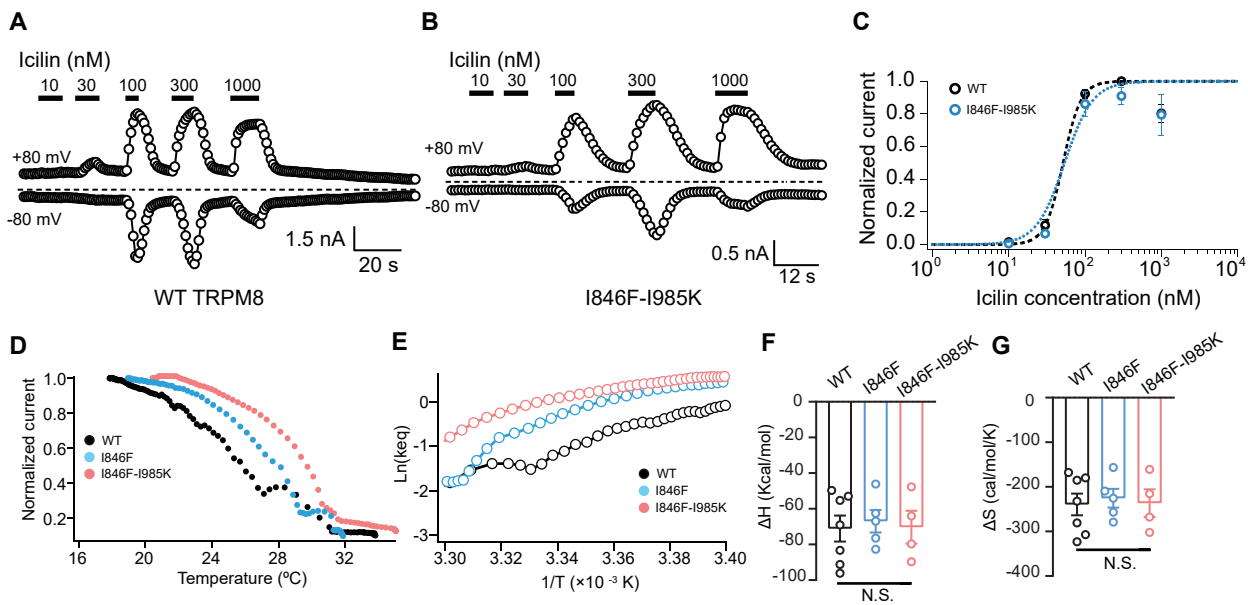
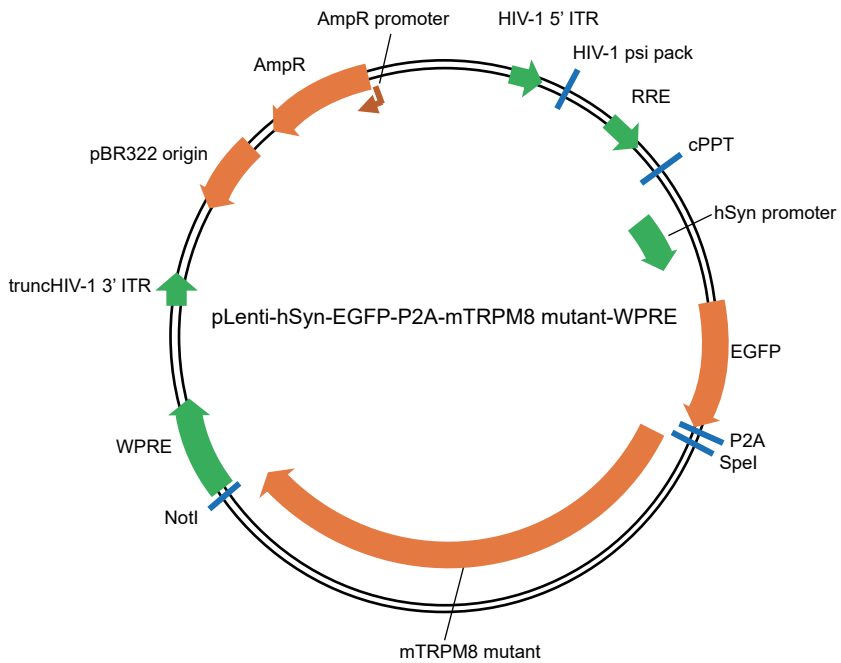


Fig. S6

**A**



**B**

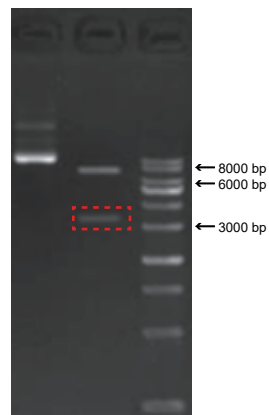
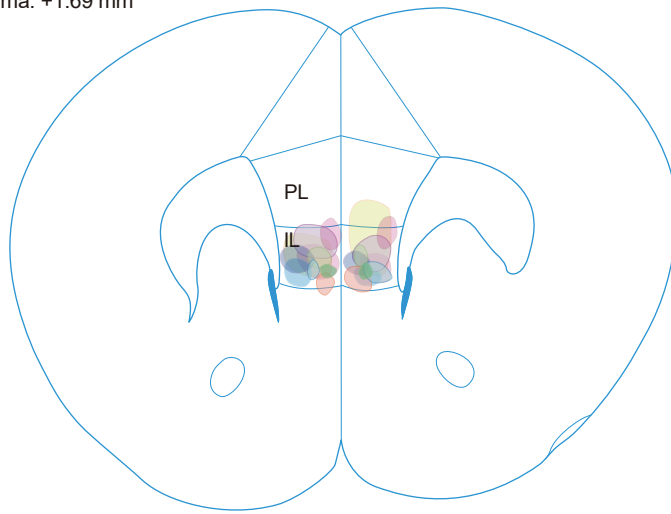
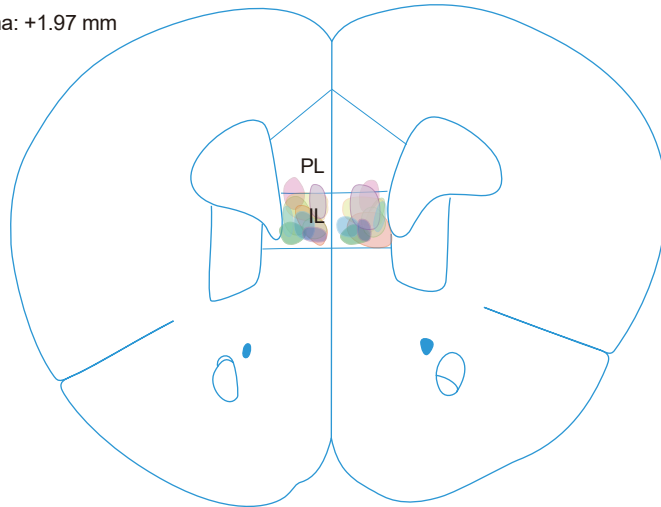


Fig. S7

bregma: +1.69 mm



bregma: +1.97 mm



bregma: -3.16 mm

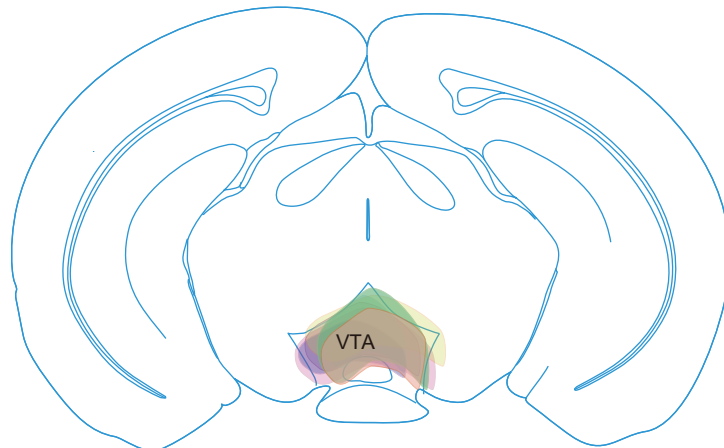


**Table. S1 Expression regions of ion channels in neural system**

Ion channel	Expression regions in neural system	references
TRPV1	Hippocampus; midbrain; cerebellum; cortex; olfactory bulb; spinal cord; intrafascicular nucleus; dorsomedial hypothalamus; posterior hypothalamus; DRG	(Roberts et al., 2004; Kim et al., 2005; Cavanaugh et al., 2011; Nam et al., 2015; Naziroglu and Ovey, 2015; Balleza-Tapia et al., 2018)
TRPV2	Hypothalamus; brainstem; spinal motor neurons; dorsal root ganglia; forebrain; cerebellum spinal cord trigeminal ganglia; DRG	(Shibasaki et al., 2010; Nilius and Flockerzi, 2014; Katanosaka et al., 2018)
TRPV3	Cortex; thalamus; trigeminal ganglia; superior cervical ganglia; cortex; dorsal spinal cord; dorsal root ganglia (monkey);	(Xu et al., 2002; Chen et al., 2022)
TRPV4	Hippocampus; cortex; cerebellum; hypothalamus; DRG	(Kauer and Gibson, 2009; Zhang et al., 2013; Zhang et al., 2017; Wang et al., 2019)
TRPA1	Hippocampus; DRG; trigeminal ganglion; nodose	(Nagata et al., 2005; Lee et al., 2016)
Kv4.2	hippocampus cerebellum and caudate putamen and thalamus	(Alfaro-Ruiz et al., 2019)
ASIC1a	DRG; olfactory bulb; cerebral cortex; hippocampus; habenula; basolateral amygdaloid nuclei; cerebellum	(Waldmann et al., 1997)
ASIC2a	Hippocampus Cortex; olfactory bulb; habenula; basolateral amygdaloid nuclei; cerebellum	(Lingueglia et al., 1997; Askwith et al., 2004)
ASIC3	Predominately expressed in PNS; detected in mesencephalic trigeminal neurons in the CNS	(Wemmie et al., 2013)
Nav1.7	Nociceptive DRG neurons; myenteric neurons; olfactory sensory neurons (OSNs); visceral sensory neurons; trigeminal ganglion neurons; thalamus; medial amygdala	(Toledo-Aral et al., 1997; Dib-Hajj et al., 2013; Branco et al., 2016; Kanellopoulos et al., 2018)
hERG	Particularly highly expressed in heart	(Pond et al., 2000)

## Reference

- 260 Alfaro-Ruiz, R., Aguado, C., Martin-Belmonte, A., Moreno-Martinez, A.E., and  
261 Lujan, R. (2019). Expression, Cellular and Subcellular Localisation of Kv4.2 and  
262 Kv4.3 Channels in the Rodent Hippocampus. *Int J Mol Sci* 20.
- 263 Askwith, C.C., Wemmie, J.A., Price, M.P., Rokhlina, T., and Welsh, M.J. (2004).  
264 Acid-sensing ion channel 2 (ASIC2) modulates ASIC1 H<sup>+</sup>-activated currents in  
265 hippocampal neurons. *J Biol Chem* 279, 18296-18305.
- 266 Balleza-Tapia, H., Crux, S., Andrade-Talavera, Y., Dolz-Gaiton, P., Papadia, D., Chen,  
267 G., Johansson, J., and Fisahn, A. (2018). TrpV1 receptor activation rescues neuronal  
268 function and network gamma oscillations from Abeta-induced impairment in mouse  
269 hippocampus in vitro. *Elife* 7.
- 270 Branco, T., Tozer, A., Magnus, C.J., Sugino, K., Tanaka, S., Lee, A.K., Wood, J.N.,  
271 and Sternson, S.M. (2016). Near-Perfect Synaptic Integration by Nav1.7 in  
272 Hypothalamic Neurons Regulates Body Weight. *Cell* 165, 1749-1761.
- 273 Cavanaugh, D.J., Chesler, A.T., Jackson, A.C., Sigal, Y.M., Yamanaka, H., Grant, R.,  
274 O'Donnell, D., Nicoll, R.A., Shah, N.M., Julius, D., *et al.* (2011). Trpv1 reporter mice  
275 reveal highly restricted brain distribution and functional expression in arteriolar  
276 smooth muscle cells. *J Neurosci* 31, 5067-5077.
- 277 Chen, X., Zhang, J., and Wang, K. (2022). Inhibition of intracellular proton-sensitive  
278 Ca(2<sup>+</sup>)-permeable TRPV3 channels protects against ischemic brain injury. *Acta*  
279 *Pharm Sin B* 12, 2330-2347.
- 280 Dib-Hajj, S.D., Yang, Y., Black, J.A., and Waxman, S.G. (2013). The Na(V)1.7

281 sodium channel: from molecule to man. *Nat Rev Neurosci* 14, 49-62.

282 Kanellopoulos, A.H., Koenig, J., Huang, H., Pyrski, M., Millet, Q., Lolignier, S.,  
283 Morohashi, T., Gossage, S.J., Jay, M., Linley, J.E., *et al.* (2018). Mapping protein  
284 interactions of sodium channel Na(V)1.7 using epitope-tagged gene-targeted mice.  
285 *EMBO J* 37, 427-445.

286 Katanosaka, K., Takatsu, S., Mizumura, K., Naruse, K., and Katanosaka, Y. (2018).  
287 TRPV2 is required for mechanical nociception and the stretch-evoked response of  
288 primary sensory neurons. *Sci Rep* 8, 16782.

289 Kauer, J.A., and Gibson, H.E. (2009). Hot flash: TRPV channels in the brain. *Trends*  
290 *Neurosci* 32, 215-224.

291 Kim, S.R., Lee, D.Y., Chung, E.S., Oh, U.T., Kim, S.U., and Jin, B.K. (2005).  
292 Transient receptor potential vanilloid subtype 1 mediates cell death of mesencephalic  
293 dopaminergic neurons in vivo and in vitro. *J Neurosci* 25, 662-671.

294 Lee, K.I., Lee, H.T., Lin, H.C., Tsay, H.J., Tsai, F.C., Shyue, S.K., and Lee, T.S.  
295 (2016). Role of transient receptor potential ankyrin 1 channels in Alzheimer's disease.  
296 *J Neuroinflammation* 13, 92.

297 Lingueglia, E., de Weille, J.R., Bassilana, F., Heurteaux, C., Sakai, H., Waldmann, R.,  
298 and Lazdunski, M. (1997). A modulatory subunit of acid sensing ion channels in brain  
299 and dorsal root ganglion cells. *J Biol Chem* 272, 29778-29783.

300 Meiler, J., and Baker, D. (2006). ROSETTALIGAND: protein-small molecule  
301 docking with full side-chain flexibility. *Proteins* 65, 538-548.

302 Miteva, M.A., Guyon, F., and Tufféry, P. (2010). Frog2: Efficient 3D conformation

303 ensemble generator for small compounds. *Nucleic Acids Res* 38, W622-627.

304 Nagata, K., Duggan, A., Kumar, G., and Garcia-Anoveros, J. (2005). Nociceptor and  
305 hair cell transducer properties of TRPA1, a channel for pain and hearing. *J Neurosci*  
306 25, 4052-4061.

307 Nam, J.H., Park, E.S., Won, S.Y., Lee, Y.A., Kim, K.I., Jeong, J.Y., Baek, J.Y., Cho,  
308 E.J., Jin, M., Chung, Y.C., *et al.* (2015). TRPV1 on astrocytes rescues nigral  
309 dopamine neurons in Parkinson's disease via CNTF. *Brain* 138, 3610-3622.

310 Naziroglu, M., and Ovey, I.S. (2015). Involvement of apoptosis and calcium  
311 accumulation through TRPV1 channels in neurobiology of epilepsy. *Neuroscience*  
312 293, 55-66.

313 Nilius, B., and Flockerzi, V. (2014). Mammalian transient receptor potential (TRP)  
314 cation channels. Preface. *Handb Exp Pharmacol* 223, v - vi.

315 Pond, A.L., Scheve, B.K., Benedict, A.T., Petrecca, K., Van Wagoner, D.R., Shrier, A.,  
316 and Nerbonne, J.M. (2000). Expression of distinct ERG proteins in rat, mouse, and  
317 human heart. Relation to functional I(Kr) channels. *J Biol Chem* 275, 5997-6006.

318 Roberts, J.C., Davis, J.B., and Benham, C.D. (2004). [3H]Resiniferatoxin  
319 autoradiography in the CNS of wild-type and TRPV1 null mice defines TRPV1 (VR-  
320 1) protein distribution. *Brain Res* 995, 176-183.

321 Shibasaki, K., Murayama, N., Ono, K., Ishizaki, Y., and Tominaga, M. (2010). TRPV2  
322 enhances axon outgrowth through its activation by membrane stretch in developing  
323 sensory and motor neurons. *J Neurosci* 30, 4601-4612.

324 Smith, C.A., and Kortemme, T. (2008). Backrub-like backbone simulation

325 recapitulates natural protein conformational variability and improves mutant side-  
326 chain prediction. *J Mol Biol* 380, 742-756.

327 Toledo-Aral, J.J., Moss, B.L., He, Z.J., Koszowski, A.G., Whisenand, T., Levinson,  
328 S.R., Wolf, J.J., Silos-Santiago, I., Halegoua, S., and Mandel, G. (1997). Identification  
329 of PN1, a predominant voltage-dependent sodium channel expressed principally in  
330 peripheral neurons. *Proc Natl Acad Sci U S A* 94, 1527-1532.

331 Valera, S., Hussy, N., Evans, R.J., Adami, N., North, R.A., Surprenant, A., and Buell,  
332 G. (1994). A new class of ligand-gated ion channel defined by P2x receptor for  
333 extracellular ATP. *Nature* 371, 516-519.

334 Waldmann, R., Champigny, G., Bassilana, F., Heurteaux, C., and Lazdunski, M.  
335 (1997). A proton-gated cation channel involved in acid-sensing. *Nature* 386, 173-177.

336 Wang, Z., Zhou, L., An, D., Xu, W., Wu, C., Sha, S., Li, Y., Zhu, Y., Chen, A., Du, Y.,  
337 *et al.* (2019). TRPV4-induced inflammatory response is involved in neuronal death in  
338 pilocarpine model of temporal lobe epilepsy in mice. *Cell Death Dis* 10, 386.

339 Wemmie, J.A., Taugher, R.J., and Kreple, C.J. (2013). Acid-sensing ion channels in  
340 pain and disease. *Nat Rev Neurosci* 14, 461-471.

341 Xu, H., Ramsey, I.S., Kotecha, S.A., Moran, M.M., Chong, J.A., Lawson, D., Ge, P.,  
342 Lilly, J., Silos-Santiago, I., Xie, Y., *et al.* (2002). TRPV3 is a calcium-permeable  
343 temperature-sensitive cation channel. *Nature* 418, 181-186.

344 Xu, L., Zhang, H., Wang, Y., Lu, X., Zhao, Z., Ma, C., Yang, S., Yarov-Yarovoy, V.,  
345 Tian, Y., Zheng, J., *et al.* (2021). De Novo Design of Peptidic Positive Allosteric  
346 Modulators Targeting TRPV1 with Analgesic Effects. *Adv Sci (Weinh)* 8, e2101716.

347 Yang, F., Xiao, X., Cheng, W., Yang, W., Yu, P., Song, Z., Yarov-Yarovoy, V., and  
348 Zheng, J. (2015). Structural mechanism underlying capsaicin binding and activation  
349 of the TRPV1 ion channel. *Nat Chem Biol* 11, 518-524.

350 Yang, S., Lu, X., Wang, Y., Xu, L., Chen, X., Yang, F., and Lai, R. (2020). A paradigm  
351 of thermal adaptation in penguins and elephants by tuning cold activation in TRPM8.  
352 *Proc Natl Acad Sci U S A* 117, 8633-8638.

353 Zhang, H., Lin, J.J., Xie, Y.K., Song, X.Z., Sun, J.Y., Zhang, B.L., Qi, Y.K., Xu, Z.Z.,  
354 and Yang, F. (2023). Structure-guided peptide engineering of a positive allosteric  
355 modulator targeting the outer pore of TRPV1 for long-lasting analgesia. *Nat Commun*  
356 14, 4.

357 Zhang, H., Sun, X., Qi, H., Ma, Q., Zhou, Q., Wang, W., and Wang, K. (2019).  
358 Pharmacological Inhibition of the Temperature-Sensitive and Ca(2+)-Permeable  
359 Transient Receptor Potential Vanilloid TRPV3 Channel by Natural Forsythoside B  
360 Attenuates Pruritus and Cytotoxicity of Keratinocytes. *J Pharmacol Exp Ther* 368, 21-  
361 31.

362 Zhang, L., Papadopoulos, P., and Hamel, E. (2013). Endothelial TRPV4 channels  
363 mediate dilation of cerebral arteries: impairment and recovery in cerebrovascular  
364 pathologies related to Alzheimer's disease. *Br J Pharmacol* 170, 661-670.

365 Zhang, N., Yang, S., Wang, C., Zhang, J., Huo, L., Cheng, Y., Wang, C., Jia, Z., Ren,  
366 L., Kang, L., *et al.* (2017). Multiple target of hAmylin on rat primary hippocampal  
367 neurons. *Neuropharmacology* 113, 241-251.